

pubs.acs.org/Macromolecules Article

Effect of Molecular Weight on Viscosity Scaling and Ion Transport in Linear Polymerized Ionic Liquids

Qiujie Zhao and Christopher M. Evans*



Cite This: Macromolecules 2021, 54, 3395-3404



ACCESS

Metrics & More

Article Recommendations

Supporting Information

Linear PILs with low dispersity (Đ<1.2)

Absolute MW determined by SEC

No electros tatic effect on viscos ity scaling of unentangled PILs

Constant morphology and decreasing σ with increasing N

ABSTRACT: A series of acrylic polymerized ionic liquids (PILs) with imidazolium cations and bis(trifluoromethylsulfonyl)imide (TFSI) anions were synthesized via reversible addition—fragmentation chain-transfer polymerization. The absolute molecular weights (MWs) of PILs were determined from size exclusion chromatography with light scattering. The degree of polymerization (N) ranged from 15 to 254, and steady rotational rheology indicated the zero-shear viscosity (η_0) measured at a constant distance above the glass transition scales as $\eta_0 \sim N^{1.0}$ for N < 92, in agreement with the theory for unentangled polymer melts. In the range from N = 92-254, we measured $\eta_0 \sim N^{2.3}$ which is interpreted as a transition region. The $N^{1.0}$ scaling in the unentangled regime is in contrast to the prior report of $\eta_0 \sim N^{1.7}$ in polyethylene-based PILs (Macromolecules, 2011, 44, 7719) but in agreement with a calculated $\eta_0 \sim N^{1.1}$ of acrylic ammonium TFSI PILs (Macromolecules, 2016, 49, 4557). Oscillatory shear rheology revealed that electrostatic interactions in this system were weak enough to have no impact on delaying the onset of flow, which was supported by a lack of ion aggregation in wide-angle X-ray scattering. The polymer nanostructure was also found to be minimally influenced by the degree of polymerization. Ionic conductivity slightly decreased as MW increased but overlapped when normalized to the calorimetric glass transition temperature.

INTRODUCTION

Polymerized ionic liquids (PILs) are a class of macromolecules with ionic liquid (IL) groups attached to the polymer backbone. They have been intensively studied in recent years due to their desirable properties such as high thermal and electrochemical stability, tunable glass transition temperature (T_{α}) and mechanical properties, and moderate ion conductivity.^{1,2} As a result, they have been demonstrated in various applications including energy-storage devices,^{3–7} gas/liquid separation membranes,^{8–13} and stimuli-responsive materials. Linear chains are the most common system for studying the impact of various parameters such as counterion type, ¹⁸⁻²¹ side chain chemistry, ^{22,23} IL placement, 24,25 ionic content, 26 and molecular weight (MW) 27,28 on PIL properties. Simulations have also elucidated these effects²⁹⁻³² and provided key insights on how the nanostructure affects polymer properties. In the vast majority of studies to date, the ionic conductivity is the metric of interest. Less work exists on other key dynamic properties and how they

depend on MW. Parameters such as viscosity and polymer center of mass diffusion will be important to understand for future applications in the context of processing, electrode adhesion, and transference number which will depend critically on not only the mobile ion diffusion but also the transport of the polyionic backbone.

The zero-shear viscosity is a key property for understanding polymer dynamics. To the best of our knowledge, only two studies have presented or mentioned the relationship between viscosity and MW in PILs. Nakamura et al.²⁷ investigated polyethylene-based imidazolium TFSI PILs and reported $\eta_0 \sim$

Received: December 18, 2020 Revised: March 18, 2021 Published: April 1, 2021





 $M_{
m v}^{1.7}$ in the unentangled regime and $\eta_0 \sim M_{
m v}^{4.2}$ in the entangled regime at $T_{
m g}$ + 35 K, where $M_{
m v}$ is the viscosityaverage MW. Classical results for neutral polymers are $\eta_0 \sim$ $M_{\rm n}^{1.0}$ and $\eta_0 \sim M_{\rm n}^{3.4}$ for unentangled and entangled polymer melts,³³ respectively. The authors attributed the larger power law factors to electrostatic interactions between the charged polymer backbone and mobile anions, although it is not obvious why such a phenomenon would have a MW dependence. Converting from viscosity to number-average MWs is not trivial, and it is unclear how these data would scale with M_n . In a separate work by Fan and coworkers, ²⁸ the viscosity scaling of acrylate-based ammonium TFSI PILs was found to be $\eta_0 \sim M_n^{1.1}$ with proper T_g normalization, which suggested that the ion interaction plays a minimal role. We noted that this scaling was not presented in the original paper but was analyzed by us using their viscosity-temperature data. To resolve these conflicting results, we hypothesize that the viscosity scalings of linear ionic polymer melts should be the same as those of neutral polymer melts, and the electrostatic interaction should not affect the scaling since zero-shear viscosity is measured in the terminal flow regime where all ionic associations are fully relaxed.

To determine the scaling laws, accurate MW determination of ionic polymers is required. PILs are typically difficult to characterize by size exclusion chromatography (SEC) due to ion aggregation and interaction with the column, leading to difficulty in measuring the degree of polymerization (N) and the MW distribution. Adding salt to the SEC solvent is a common strategy to screen the charges and reduce the polymer-column interaction. Early MW measurements of PIL homopolymers used dimethylformamide (DMF) with LiBr salt as the elution mixture and were calibrated against polyethylene oxide (PEO) standards. The work by Lee et al.³⁴ found that an acrylate-based imidazolium TFSI PIL, made by free-radical polymerization, had an $M_n = 6.65$ kDa and a dispersity (D) of 2.4 when eluted with DMF + 0.05 M LiBr. The refractive index (RI) signal showed a broad, two-hump elution peak, suggesting either inhomogeneous polymerization or strong interaction between the ionic polymer and the SEC column. Subsequent work by Ye and Elabd³⁵ investigated a series of methacrylatebased imidazolium PILs with five different anions using the same solvent and compared the MW data calibrated with PEO and polystyrene (PS) standards. The reported dispersity (D) ranged from 2.45 to 2.77 against PEO standards while D =1.21–1.32 against PS standards, highlighting the perils of citing dispersity values against relative MW standards to infer the real MW distributions of ionic polymers. Nevertheless, calibration against known standards is easy to perform and only requires a RI detector, hence the wide spread use of this method. 36-41 A more detailed study on the SEC conditions for PILs⁴² found that DMF and tetrahydrofuran with 10 mM LiTFSI appear to work for styrenic TFSI PILs, resulting in "normal" SEC peaks and the authors were able to construct a calibration curve using a separate batch of PIL standards to obtain the absolute MWs. Alternatively, some studies analyzed the uncharged precursor polymers and assumed the same N following functionalization and ion exchange. ^{28,42,43} Ideally, absolute MW determination is needed to probe scaling relations which has been determined for ammonium bromide ionenes44 using a mixture of water, methanol, acetic acid, and sodium acetate. The quantity of each component was carefully tuned to minimize polymer aggregation and polymer-column interaction. Monomodal SEC curves were observed, and the measured MW correlated

well with the stoichiometry of the two monomers, as well as the polymerization time.

Due to the low polarity of most polymer matrices, ion pairs tend to aggregate $^{45-47}$ and generate ionic cross-links that can impact both conductivity and rheological behaviors. 48 Recently, the effect of MW on PIL aggregation has been studied⁴⁹ by wide-angle X-ray scattering (WAXS), with Nranging from 2 to 109. The authors found that the positions of three scattering peaks, which correspond to the amorphous halo, anion correlation, and intercluster scattering from highto-low wave vector (q), were invariant for N > 10. However, the low q ion aggregation peak was not observable for the dimer and the trimer which was attributed to the lack of structural periodicity. 49 Similarly, ion transport in PILs was less-affected by MW once N exceeds some critical value. This is evident in a previous report²⁸ where the PIL ionic conductivity overlapped for \tilde{N} above 10. This work also showed that the degree of decoupling between ion transport and segmental dynamics was the same once the PIL had sufficient repeating units (N > 10). While conductivity appears to be minimally affected, the clustering of ions at the nanoscale is potentially more important in determining chain level dynamics depending on how many clusters per chain are formed.

In this work, we synthesized a series of linear imidazolium TFSI PILs with an acrylate backbone and a range of N from 15 to 254 via controlled radical polymerization to achieve low dispersity. The MW was determined by SEC with multiangle light scattering (MALS). The viscoelastic properties were characterized by both oscillatory and rotational shear rheology, and zero-shear viscosity was extracted at $T_{\rm g}$ + 43 K for comparison. The viscosity-MW scaling relationship in the unentangled regime was found to be $\eta_0 \sim M_n^{1.0}$, which confirmed the hypothesis that electrostatic interactions have no effect on viscosity scaling for this system. The power law increased to 2.3 in the transition region as N increased but did not reach the fully entangled regime due to synthetic difficulty in pushing to higher N. The nanostructure inferred from WAXS was not affected by increasing MW, and $T_{\rm g}$ normalization allows for conductivity to superpose suggesting that ion conduction was similarly coupled to segmental dynamics across this broad range of MWs.

MATERIALS AND METHODS

Materials. Acryloyl chloride (97%, 200 ppm MEHQ stabilizer), 3bromo-1-propanol (97%), 1-methylimidazole (99%), 2,2'-azobis(2methylpropionitrile) (AIBN, 99%, recrystallized), N,N-dimethylformamide (DMF, anhydrous, 99.8%), butylated hydroxytoluene (BHT, ≥99%, FCC, FG), and lithium bis(trifluoromethanesulfonyl)imide salt (LiTFSI, 99.95%) were purchased from Sigma-Aldrich and used as received. Cyanomethyl dodecyl trithiocarbonate (98%) was purchased from Sigma-Aldrich and Strem Chemicals. Methanol (HPLC grade), glacial acetic acid (HPLC grade), sodium acetate (anhydrous, >99%), diethyl ether (ACS grade, BHT stabilized), hexane (ACS grade), ethyl acetate (ACS grade), and triethylamine (Et₃N, 99%) were purchased from Fisher Scientific and used as received. Dichloromethane (DCM, stabilized, HPLC grade) was purchased from Fisher Scientific and dried with molecular sieves prior to use. Deionized water (DI H2O) was acquired from a Millipore Ultrapure water system. Dialysis bags with 1 kDa molecular weight cutoff (MWCO) were purchased from Spectrum Labs.

Synthesis of 3-Bromopropyl Acrylate. 3-Bromopropanol (4.94 g, 35.6 mmol) was dissolved in 20 mL of DCM in an oven-dried, nitrogen-purged flask. The solution was cooled to 0 °C and acryloyl chloride (3.38 g, 37.3 mmol) dissolved in 20 mL of DCM was added.

Scheme 1. Synthesis of Linear TFSI PILs Using RAFT Polymerization Followed by Ion Exchange

Next, triethylamine (4.32 g, 42.7 mmol) dissolved in 20 mL of DCM was added dropwise with stirring. The reaction mixture was allowed to recover to room temperature and stirred for 4 h. The mixture was purified by silica gel flash chromatography (25:1 hexane/ethyl acetate, $R_{\rm f}=0.2$). The fractions were collected, and 6 mg (~0.1 mol %) of BHT was added to stabilize the acrylate. The product was concentrated under reduced pressure to afford a clear liquid (6.68 g, 97% yield). ¹H NMR (CDCl₃, 500 MHz): δ (ppm) 6.43 (CH₂=CH-, d, 1H), 6.12 (CH₂=CH-, q, 1H), 5.86 (CH₂=CH-, d, 1H), 4.31 (-CH₂-CH₂-O-, t, 2H), 3.49 (Br-CH₂-CH₂-, t, 2H), 2.23 (-CH₂-CH₂-CH₂-, p, 2H)

Synthesis of 1-(3-(Acryloyloxy)propyl)-3-methyl-imidazolium Bromide (Br IL). 3-Bromopropyl acrylate (4.11 g, 21.3 mmol), methylimidazole (2.62 g, 31.9 mmol), and BHT (19.4 mg, 0.088 mmol) were dissolved in 10 mL of anhydrous DMF and purged with nitrogen for 20 min. The reaction mixture was stirred at 35 °C for 24 h and precipitated in 200 mL of diethyl ether three times to remove the solvent and unreacted compounds. The viscous precipitate was collected using DCM, and the solution was concentrated under reduced pressure to afford a clear viscous liquid (4.26 g, 73% yield). 1 H NMR (CDCl₃, 500 MHz): δ (ppm) 10.5 (Im $^+$, s, 1H), 7.54 (Im $^+$, s, 1H), 7.48 (Im $^+$, s, 1H), 6.41 (CH₂=CH $^-$, d, 1H), 6.10 (CH₂=CH $^-$, q, 1H), 5.87 (CH₂=CH $^-$, d, 1H), 4.51 ($^-$ CH₂-CH $^-$, $^-$ CH $^-$, s, 3H), 2.38 ($^-$ CH₂-CH $^-$, p, 2H).

Synthesis of Poly(1-(3-(acryloyloxy)propyl)-3-methyl-imidazolium Bromide) (Br PlL). The polymerization of the Br IL monomer was achieved using reversible addition—fragmentation chain-transfer (RAFT) polymerization. For an example synthesis of 10 kDa Br PIL, Br IL monomer (0.57 g, 2.08 mmol), cyanomethyl dodecyl trithiocarbonate (18.1 mg, 0.057 mmol), and AIBN (3.8 mg, 0.023 mmol) were dissolved in 2 mL of anhydrous DMF in a Schlenk flask. The solution was freeze—pump—thawed three times and heated at 70 °C for 24 h. After the reaction, the mixture was precipitated in 50 mL of diethyl ether three times, and the polymer was collected and vacuum-dried at 70 °C for 12 h to afford a white-yellow solid (0.51 g, 89% yield).

Synthesis of Poly (1-(3-(acryloyloxy)propyl)-3-methyl-imidazolium Bis(trifluoromethane-sulfonyl)imide) (TFSI PIL). PILs with TFSI anions were prepared by ion exchange. As an example, dried Br PILs (0.29 g, 1.05 mmol Br $^-$) and LiTFSI (3.05 g, 10.6 mmol, \sim 10 equiv) were dissolved in 10 mL of methanol separately and two solutions were mixed in the 1 kDa MWCO dialysis bag and dialyzed against 500 mL of 1:1 (v/v) methanol/water mixture. This large excess of LiTFSI is needed, as shown in our prior work on PIL ion exchange. So A fresh solvent mixture was switched every day and the ionic conductivity of the dialysate was monitored until it reached 2 μ S/cm or below. The polymer was collected and vacuum-dried at 100 °C for 24 h and stored in an argon glovebox for further use.

Elemental analysis was performed to determine the fluorine and the residue bromine contents in the TFSI PILs.

Thermal Characterization. The glass transitions of the TFSI-anion PILs were measured using a TA instruments DSC2500 differential scanning calorimeter with a 10 °C/min heating/cooling rate between -50 and 150 °C. The glass transition temperature (T_g) was determined from the second heating curve using the 1/2 ΔC_p method.

Dynamic Light Scattering. Dynamic light scattering (DLS) measurements were performed on Br PILs dissolved in the SEC solvent mixture to check the polymer aggregation behavior. The data were collected on a Malvern Zetasizer Nano-ZS series equipped with a 633 nm He-Ne laser operating in the 175° backscattering mode. The solutions were equilibrated at 50 °C for 5 min before measurements, and average data from three consecutive DLS runs were reported.

MW Characterization. The absolute MWs of Br PILs were determined using a Tosoh EcoSEC Elite Model HLC-8420, equipped with two Tosoh TSKgel Alpha-M columns, a Tosoh Dual-Flow RI detector, and a Tosoh LenS3 MALS detector. The elution solvent was a mixture of water, methanol, and acetic acid (55:23:23 by volume ratio) with 0.54 M sodium acetate (measured pH = 4.06), which was previously reported for successful MW determination of Br ionenes.⁴⁴ The bulk solvent was prepared and filtered through two layers of 0.22 µm nylon disc filters (Thomas Scientific) under low vacuum to remove any impurities. The polymers were dissolved at room temperature for at least 3 h and filtered through 0.45 μm Teflon syringe filters (Fisher Scientific). The sample concentrations were 2-14 mg/mL depending on the PIL MW, and the injection volumes were 50 μL . The flow rate was 0.6 mL/min, and the column temperature was 50 °C. A narrow polydispersity index (PDI) poly(ethylene oxide) (PEO) standard (20.9 kDa, PDI = 1.04, PolyAnalytik) was used for detector calibration and elution time correction. A dextran standard (74.8 kDa, PDI = 1.31, PolyAnalytik) was used for MW validation. Seven PEO standards (23.6-903 kDa, Tosoh) were used for conventional calibration. The data were processed using Tosoh SECview software.

Nuclear Magnetic Resonance. The intermediate compounds, IL monomers, and Br PILs were measured at room temperature on either U500 or VXR500 spectrometer, and the TFSI PILs were measured on a CB500 spectrometer. The end group analysis on TFSI PILs was conducted on baseline and phase-corrected spectra by integrating and comparing the imidazolium protons (1H per monomer, ~9 ppm) and the CH₃ protons on the RAFT chain end (3H per chain, 0.8–0.9 ppm).

Wide-Angle X-ray Scattering. The ionic aggregate morphology was characterized using transmission WAXS. The WAXS setup is composed of a Xenocs GeniX3D Cu K α X-ray source (1.54 Å) and a Pilatus 2D detector. A rod beam stop was placed in front of the

detector to attenuate the primary beam. The sample-to-detector distance was calibrated with silver behenate. All samples were lined up on the same sample holder and the scattering patterns were collected with a 30 min exposure time on each sample under ambient conditions. The 2D diffraction data were processed using FIT2D software, and the intensity was plotted as a function of scattering vector \boldsymbol{q} .

Ionic Conductivity Measurements. The ionic conductivities of TFSI PILs were measured using electrochemical impedance spectroscopy. All samples were prepared in an argon glovebox. Each polymer was placed in between two stainless-steel electrodes with a Kapton spacer. The assembly was put into a sample holder (Bio-Logic CESH) and connected to a potentiostat (Bio-Logic SP-300) under nitrogen purging. The sample was first heated to 70 °C and equilibrated for at least 1.5 h. Then, the impedance spectra were collected from 70 $^{\circ}$ C to near $T_{\rm g}$ with a 5 K interval and a 30 min equilibration time. The applied voltage was 100 mV, and the frequency range was 106 Hz to 10⁻¹ Hz. The sample thickness was checked before and after the measurement to ensure no significant deformation. The impedance data were processed to make a plot of real (σ') and imaginary (σ'') conductivities versus frequency. The ionic conductivity was taken as the real conductivity at the $tan(\delta)$ = σ'/σ'' maximum.

Shear Rheology. The viscoelastic properties of TFSI f-PILs were measured using a stress-controlled rheometer (TA instruments DHR-2) equipped with an environmental chamber and an 8 mm parallel-plate geometry. The polymer was loaded at 110 °C under nitrogen and equilibrated for 1 h. Then, frequency sweeps were performed every 10 °C between 50 °C and near $T_{\rm g}$, as well as at $T_{\rm g}$ + 43 K. The polymer was allowed to equilibrate in the chamber for 10 min at each temperature before shear experiments. Torque/stress sweeps were performed prior to frequency sweeps to ensure linear response from the polymer. Additional flow curve measurements (viscosity vs shear rate) were conducted at $T_{\rm g}$ + 43 K to measure the zero-shear viscosity. The reported η_0 values were averaged from at least two repeated runs. Data were processed using TA instruments TRIOS software.

RESULTS AND DISCUSSION

PIL Synthesis. Linear PILs were synthesized via RAFT polymerization (Scheme 1). Briefly, 3-bromo-1-propanol was first reacted with acryloyl chloride to form a polymerizable acrylate group. The bromine end was converted into imidazolium bromide by quaternization with 1-methylimidazole. The ionic acrylate monomer was polymerized with a trithiocarbonate RAFT agent, and the MW was controlled by the ratio of monomer to RAFT agent. At very high MW, Br PILs tended to precipitate out of solvent, and the highest degree of polymerization investigated was N = 254. The Br anions were ion-exchanged to TFSI anions with a large excess of LiTFSI (10 equiv based on our prior studies of exchange conditions)50 and extensive dialysis to minimize residual Br content, which was found to be less than 0.1 wt % by elemental analysis (Table S1). The final dried TFSI PILs had glass transition temperatures ranging from -19 to -12 °C. The T_g versus N relationship was well-described using the Fox-Flory equation (Figure S1)

$$T_{g}(N) = T_{g,\infty} - \frac{B}{N} \tag{1}$$

where $T_{\rm g,\infty}$ is the plateau glass transition temperature and B is an empirical parameter. The majority of our TFSI PILs had $T_{\rm g}$ close to the plateau $T_{\rm g}$ (13 °C).

MW Characterization. The MW was first obtained by analyzing the Br PILs via SEC. The elution solvent was a mixture of water, methanol, and acetic acid (54:23:23 by volume) with 0.54 M sodium acetate, which was adapted from

a previous report by Layman and co-workers.⁵¹ This solvent mixture dissolved Br PILs well, and no polymer aggregation was found in the solution based on DLS measurements (Figure S2). The TFSI PILs, on the other hand, were not soluble in this aqueous mixture due to the hydrophobic nature of TFSI anions. A solvent of DMF with 10 mM LiTFSI, which worked well for styrenic imidazolium TFSI PILs,⁴² was not suitable for the acrylate PILs in this study.⁵² Hence, SEC was performed on the Br form to determine *N* values and MW distributions, which change little upon exchange to the TFSI form. The ion exchange was performed in a 1 kDa MW cutoff dialysis bag to minimize polymer loss, and end group analysis of the TFSI polymer by nuclear magnetic resonance (NMR) provides good agreement with the initial Br polymers. One representative SEC curve with an RI signal is shown in Figure 1. The RI peak

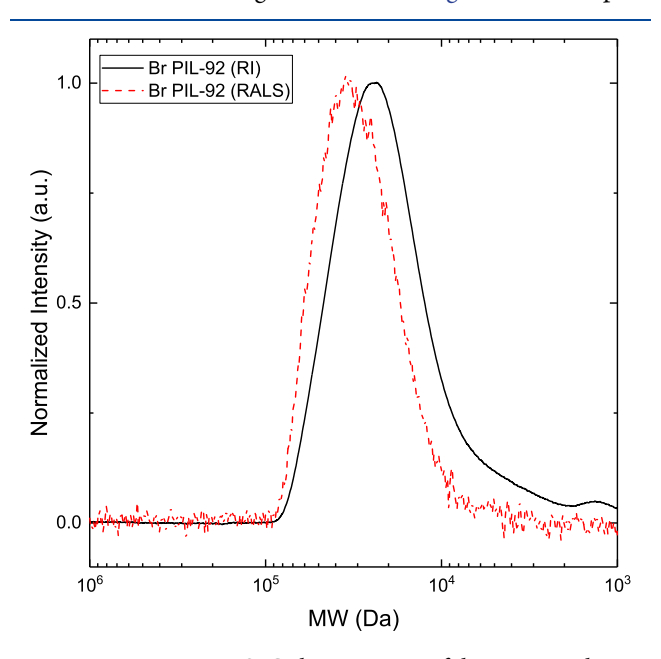


Figure 1. Representative SEC chromatogram of the Br PIL with $M_{\rm n}$ = 25.4 kDa (N = 92), showing the signals of RI and RALS. The MW on the x-axis was derived from the RALS signal.

was relatively symmetric with a slight tail at lower MW, possibly due to a small fraction of oligomeric PILs. A more symmetric SEC peak was observed for the light-scattering signal measured at 90° angle (i.e., right-angle light scattering, RALS). The peak positions between RI and LS signals were offset, possibly due to the detector sensitivity. The RI detector is sensitive to concentration, so polymer fractions in the middle of the MW distribution that have the highest concentration will give the strongest RI response. The LS detector is sensitive to both concentration and MW, so polymer fractions at the high end of the MW distribution will provide the highest scattering intensity. SEC curves of all samples were plotted for each detector and are shown in the Supporting Information (Figures S3–S6). The signal-to-noise ratios were good for all four detectors except for low angle (10°), which is potentially due to low polymer concentrations and the close proximity of the elution line and the scattered light. The MW information of Br PILs derived from LS distribution measured at 90° angle is summarized in Table 1. The samples will be referred as "PIL-N" for the rest of the paper, where N is the degree of polymerization derived from number-average MW (M_n) of Br PILs measured by SEC.

Table 1. Summary of MW Distributions of Br PILs from SEC, Degree of Polymerization of TFSI PILs from NMR End Group Analysis, and T_g of TFSI PILs from DSC

sample: PIL-X ^a	Br PILs			TFSI PILs	
	M _{n,Br(SEC)} (kDa)	M _{w,Br(SEC)} (kDa)	$D_{\mathrm{Br(SEC)}}$	N _{TFSI(NMR)}	T _{g,TFSI} (°C
PIL-15	4.3	4.4	1.02	15	-18
PIL-19	5.1	5.4	1.07	23	-19
PIL-31	8.4	9.6	1.15	46	-16
PIL-92	25.4	29.2	1.15	98	-15
PIL-115	31.7	36.8	1.16	119	-13
PIL-123	33.9	39.7	1.17	158	-14
PIL-162	44.7	52.0	1.16	159	-12
PIL-192	52.7	63.2	1.20	271	-14
PIL-254	69.8	85.8	1.23	290	-13

 aX is the degree of polymerization calculated from $M_{\rm n,Br(SEC)}$ $(X = M_{\rm n,Br(SEC)}/MW_{\rm Br~IL})$.

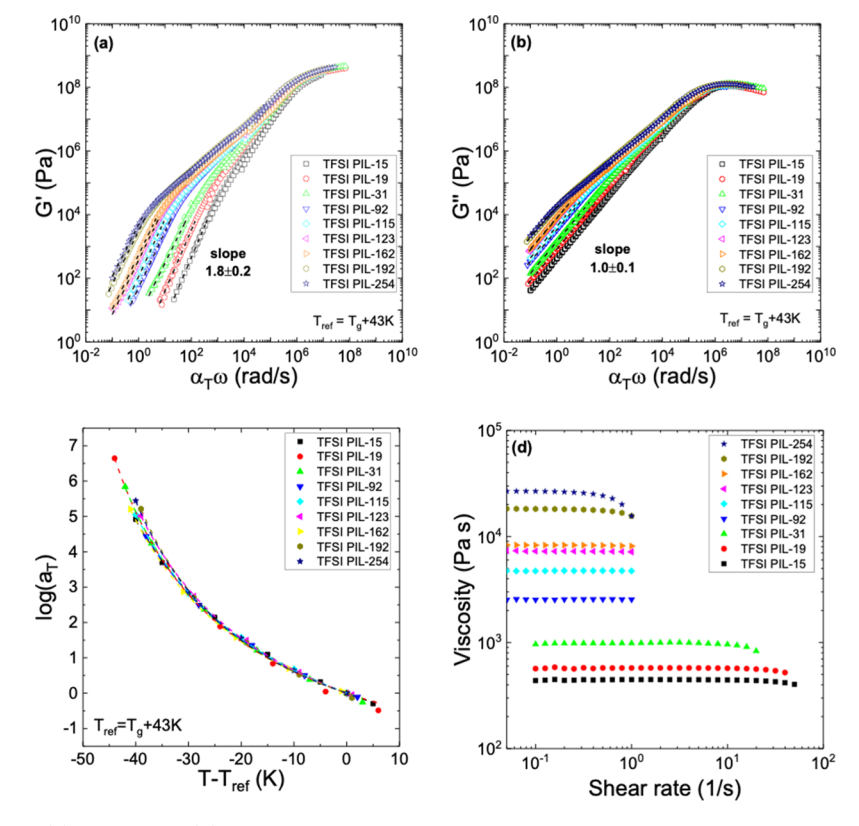


Figure 2. Horizontally shifted (a) storage and (b) loss modulus of TFSI PILs based on frequency sweep data from 30 °C to near $T_{\rm g}$: $T_{\rm ref} = T_{\rm g} + 43$ K. (c) Horizontal shift factors ($\alpha_{\rm T}$) vs $T - T_{\rm ref}$: Data were fitted with the WLF equation. (d) Viscosity of TFSI PILs vs shear rate at $T_{\rm g} + 43$ K. Zeroshear viscosities were calculated by averaging the data in the plateau regions.

The Br PILs exhibited narrow MW distributions with dispersity ranging from 1.02 to 1.23 because of the controlled nature of RAFT polymerization. The low D is helpful in minimizing dispersity effects on viscoelastic properties, which was known to broaden the relaxation spectrum in the terminal region and alter the viscosity response of polymer melts. S3-56 When comparing the degrees of polymerization calculated from $M_{\rm n,Br}$ and from NMR analysis on TFSI PILs (Figure S7), there is a good agreement across the studied MW range. At higher MWs (N > 162), deviations are observed, which is expected as end group analysis becomes less accurate. Therefore, MW information from SEC was used for subsequent analyses.

Rheological Characterization and Viscosity-MW Scaling. The effect of MW on viscoelasticity of TFSI PILs was

characterized by conducting oscillatory and rotational shear rheology. Time—temperature superposition (TTS) was successfully applied to frequency sweep data of TFSI PILs with $T_{\rm ref} = T_{\rm g} + 43$ K. The shifted moduli data were plotted in Figure 2a,b. The data showed that the loss modulus (G') was always higher than the storage modulus (G') except near the glass transition. With increasing N, a systematic shift of the terminal region to lower frequency was observed, consistent with the emergence of entanglements which become more prominent as the MW increases. At low MWs (N = 15, 19, and 31), a rubbery plateau is not observed, suggesting that the imidazolium and TFSI ion pairs do not form strong enough physical cross-links to perturb the rheology. This is also supported by the absence of ion aggregation peaks in WAXS measurements, which will be discussed later. The scaling of G'

in the terminal regime was $G' \sim \omega^{1.8\pm0.2}$, slightly lower than the characteristic $\omega^{2.0}$ scaling, while $G'' \sim \omega^{1.0\pm0.1}$ as anticipated. The temperature dependence of horizontal shift factors $(\alpha_{\rm T})$ is shown in Figure 2c, and the data overlapped on a $T_{\rm g}$ -normalized scale. The shift factor was analyzed using the Williams—Landel—Ferry (WLF) equation

$$\log(a_{\rm T}) = \frac{-C_{\rm l}(T - T_{\rm ref})}{C_{\rm 2} + T - T_{\rm ref}}$$
(2)

where C_1 and C_2 are empirical constants. The values are tabulated in Table S2. C_1 and C_2 remained relatively constant in the studied MW range. We also shifted the frequency data to a fixed temperature ($T_{\rm ref} = 30$ °C, Figure S8) and found that the shift factors at low temperature systematically increased with decreasing MW due to the increase in $T_{\rm g}$.

Flow curves of TFSI PILs were measured at $T_{\rm g}$ + 43 K (Figure 2d), and η_0 was obtained from the plateau region. The experiments started from low shear rates and were stopped when nonlinear behavior was observed (i.e., viscosity decreased). The effect of MW on zero-shear viscosity of TFSI PILs is illustrated in Figure 3, where η_0 was plotted

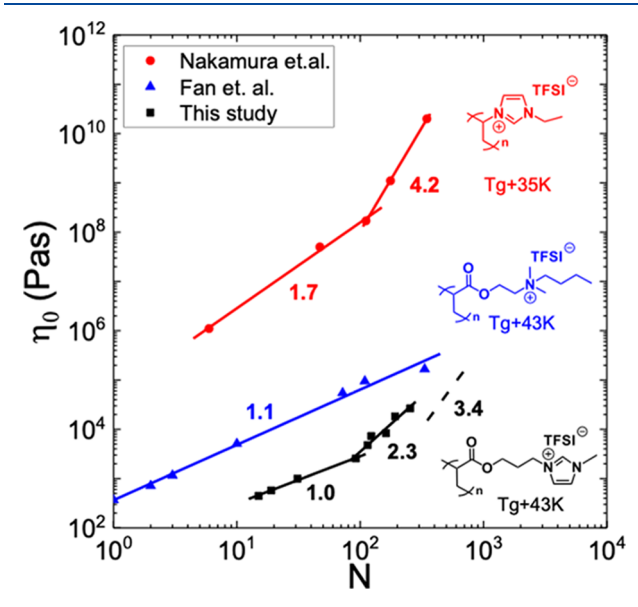


Figure 3. Effect of MW on $T_{\rm g}$ -normalized zero-shear viscosity of three TFSI PILs. The plot includes viscosity vs viscosity-average $N_{\rm v}$ at $T_{\rm g}$ + 35 K from Nakamura et al. (red circles), viscosity vs number-average N at $T_{\rm g}$ + 43 K from Fan et al. (blue triangles), and viscosity vs number-average N at $T_{\rm g}$ + 43 K from this study (black squares). The scaling factors (number below solid lines) and PIL structures are shown. The 3.4 scaling factor (dash line) was drawn to illustrate the anticipated scaling in the entanglement regime.

against N derived from SEC measurements. We observed two distinct regions. Below N=92, $\eta_0\sim N^{1.0\pm0.1}$, which corresponds to the unentangled regime. This is consistent with the scaling of neutral polymer melts. Above N=92, $\eta_0\sim N^{2.3\pm0.3}$, which is lower than the well-known $N^{3.4}$ for entangled polymer melts. We attribute the 2.3 power law to a transition region where the polymers are not fully entangled. The zero-shear viscosity data were also plotted against $N_{\rm TFSI}$ from NMR end group analysis, and the scaling factors are the same within fitting errors (Figure S9).

Viscosity scaling relations from two previous PIL studies were analyzed and compared with the present work. Zero-

shear viscosities of five polyethylene-based imidazolium TFSI PILs from Nakamura et al. 27 were measured at $T_g + 35$ K and plotted against viscosity-average degree of polymerization $N_{\rm v}$. The authors found power law exponents of 1.7 (unentangled) and 4.2 (unentangled), compared to 1.0 and 3.4 for neutral polymer melts. They attributed the higher scaling factors to electrostatic interactions between polymer chains and counterions.²⁷ In a separate work by Fan et al.²⁸ which looked at the acrylate-based ammonium TFSI PILs with different MWs, the viscosity scaling relationship was not explicitly discussed, but we were able to use the reported Vogel-Fulcher-Tammann (VFT) fit parameters to calculate PIL viscosities at T_{α} + 43 K (Table S3) to compare with our zero-shear viscosity data. The degree of polymerization in this case is a number-average N, and we found that the viscosity scaling was $N^{1.1}$ throughout the entire N range. This scaling factor is similar to what we observed and followed the expectation from the sticky Rouse model (see Supporting Information for derivations). 57,58 The key differences among the three scaling studies are the PIL design and determination of MWs. Free radical polymerization was used by Nakamura and co-workers and the MW was determined by viscometry.²⁷ No dispersity was reported, but it is expected to be larger than PILs obtained by controlled radical polymerization. In addition, M_v of PILs in that study were determined using Mark-Houwink parameters of PS in methyl ethyl ketone. Although the solvent and temperature conditions for solution viscometry were the same between PS and PILs, and additional salt was added to PIL solution to reduce aggregation, it is not clear if the conformation of the charge-screened PIL is the same as that of PS. In the work of Fan et al.,²⁸ RAFT polymerization was used to achieve low D (<1.2) and M_n was determined from the unquaternized polymer precursors. In the present study, polymers were also made by RAFT, and absolute MWs were measured using light scattering and SEC on the intermediate Br PILs and the N values corresponded well with that of TFSI PILs. It is also worth noting that the ammonium PILs did not show any indication of entanglement even at N = 333, while two imidazolium PILs appeared to show the emergence of entanglement effects above $N \sim 100$. Such a variation in the critical degree of polymerization (N_c) for the onset of entanglements has been observed in neutral polymer melts, for example, $N_c = 337$ for PS and $N_c = 124$ for polybutadiene.³³ This may be related to a difference in persistence length of the chains with different side groups, but further work is needed. Another important observation is the vast difference in viscosity of three different PIL structures even when they were all normalized to T_g + 35 K (Figure S10). To obtain this data, we also calculated the zero-shear viscosity of our PILs using the G'' master curves with $T_{ref} = T_g + 35 \text{ K}$ and the following relation

$$\eta_0 = \lim_{\omega \to 0} \frac{G''}{\omega} \tag{3}$$

The viscosity data in the present work and those of Fan et al. 28 were shifted up compared to Figure 3 to account for the difference between $T_{\rm g}$ + 43 K and $T_{\rm g}$ + 35 K. The MW scaling factors were consistent between shear and rotational experiments. However, the viscosities of the two acrylate-based PILs were still 2–4 orders of magnitude lower than that of the polyethylene-based PIL, and the ammonium acrylates were more viscous than imidazolium acrylates with a similar side chain length, suggesting that strong intermolecular interactions

can come from either a rigid backbone or stronger ionic interactions.

PIL Morphology. The effect of MW on PIL nanostructure was investigated using WAXS (Figure 4). The assignments of

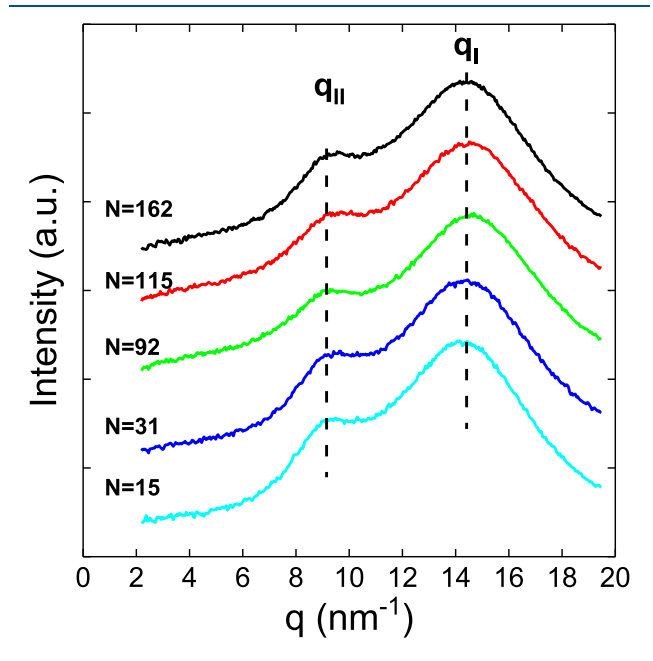


Figure 4. WAXS patterns of five TFSI PILs with increasing MW (from bottom to top). The curves were vertically shifted for clarity. The middle $q_{\rm II}$ peak (~9 nm⁻¹) is the anion–anion correlation peak and the high $q_{\rm I}$ peak (~14 nm⁻¹) is the amorphous halo.

PIL scattering peaks were presented in prior reports based on both experimental and simulation studies. 18,20,59,60 The high q peak corresponds to the amorphous halo of the polymer ($q_{\rm I}=14.4\pm0.1~{\rm nm}^{-1}$) and the intermediate peak reflects the anion—anion correlations ($q_{\rm II}=9.2\pm0.1~{\rm nm}^{-1}$). With increasing MW, the correlation peak positions remained the same. The characteristic low q peak at \sim 4 nm⁻¹ which corresponds to intercluster ionic aggregates was not observed in this system. This indicates that the extent of ion aggregation was too weak to show significant scattering correlations and is consistent with the rheology data where no obvious ionic cross-link plateau was observed. This low extent of aggregation

is attributed to weak ionic interactions between imidazolium cations and TFSI anions, as well as low fraction of nonpolar groups, which was also found in 1-propyl-3-methylimidazolium TFSI ${\rm IL}$, 61 a small-molecule analogue to our PILs. Thus, increasing MW had no discernible effect on PIL morphology in the studied N range.

lonic Conductivity. The ionic conductivity of TFSI PILs with varying MW was measured from 70 °C to near $T_{\rm g}$ (Figure 5a). The ionic conductivity decreased as temperature decreased, which is typical for ionic polymers due to a reduction in segmental dynamics. In addition, the conductivity at a fixed temperature was reduced with increasing MW, which is likely due to the difference in $T_{\rm g}$. After the data were normalized by $T_{\rm g}$ (Figure 5b), the ionic conductivities among different PILs are approximately the same. The data were well-described using the VFT equation

$$\sigma = \sigma_{\infty} \exp\left(-\frac{DT_0}{T - T_0}\right) \tag{4}$$

where σ_{∞} is the theoretical high-temperature conductivity, D is the VFT strength parameter, and T_0 is the reference temperature at which conductivity drops to infinitesimal. The fit parameters are summarized in Table S4. The strength parameter, which reflects the rate of conductivity reduction as temperature decreases, is approximately independent of the MW. The reference temperature T_0 tracked with glass transition temperature where the difference $T_g - T_0$ remained nearly constant. This indicates that ion conduction is coupled to the segmental dynamics to a similar degree within the studied N range. This is in agreement with the previous report that conductivities of TFSI PILs exhibited very small variations when N changed from 10 to 333.

CONCLUSIONS

In conclusion, we systematically studied the effect of degree of polymerization, ranging from 15 to 254, on the dynamic properties and nanostructure of linear imidazolium TFSI PILs. The polymers were synthesized via controlled radical polymerization to achieve low dispersity, and MW information was obtained using SEC with water/methanol/acetic acid/sodium acetate as the solvent mixture. In-line MALS was successfully applied to obtain absolute MWs without the need of relative standards such as PEO. The number-average MW from SEC

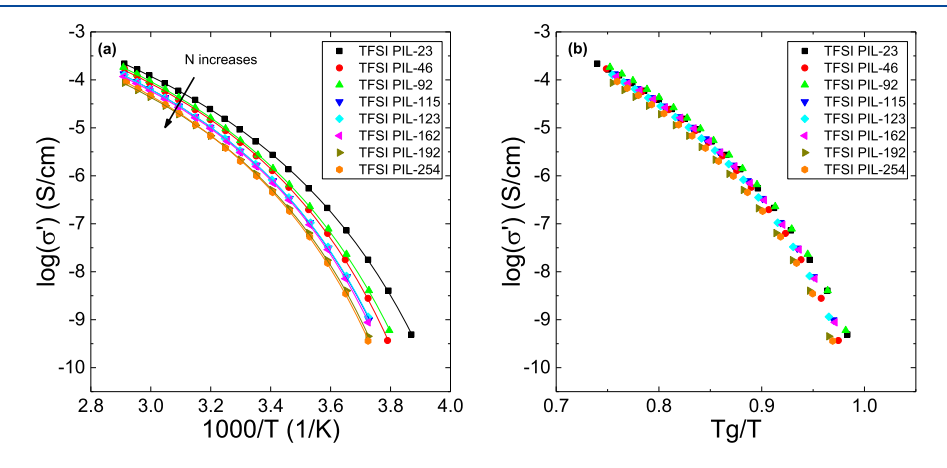


Figure 5. (a) Ionic conductivity as a function of temperature of TFSI PILs from 70 $^{\circ}$ C to near $T_{\rm g}$. (b) $T_{\rm g}$ -normalized ionic conductivity of TFSI PILs.

and NMR end group analysis is consistent, except for the largest samples where NMR accuracy decreases. Oscillatory and rotational shear rheology were used to measure the viscoelastic properties of the TFSI PILs, and TTS worked well in the frequency sweep data. Flow curves were analyzed to give zero-shear viscosities which showed $\eta_0 \sim N^{1.0}$ below N = 92, consistent with expectations of unentangled polymer melts according to the sticky Rouse model and in agreement with our analysis of data from Fan et al. 28 Above N = 92, deviations from this scaling were observed as $\eta_0 \sim N^{2.3}$ and did not reach the value expected for fully entangled polymers. The rheology of unentangled PILs indicated that electrostatic interactions have a minimal effect on the PIL viscoelasticity for the present imidazolium-TFSI polymers. WAXS measurements showed no ionic aggregation peak in the low wave vector region, suggesting a minimal extent of ion clustering and supporting the observation that there is no ionic cross-link plateau in the TTS curves. In addition, no significant change in correlation peaks was observed with increasing MW in the studied N range. Finally, ionic conductivity of PILs at a given temperature slightly decreased as MW increased, but when the temperature was normalized by T_g , the data overlapped. This is consistent with the idea that ion transport is coupled to more local dynamics and is not sensitive to chain level processes.

ASSOCIATED CONTENT

Solution Supporting Information

The Supporting Information is available free of charge at https://pubs.acs.org/doi/10.1021/acs.macromol.0c02801.

 $T_{\rm g}$ vs N plot, DLS data, SEC elution curves, representative NMR spectrum for end group analysis, modulus master curves at $T_{\rm ref}=30$ °C, WLF fit parameters, calculations of PIL viscosities from ref 27, and VFT fit parameters for ionic conductivity and viscosity scaling derived from the sticky Rouse model (PDF)

AUTHOR INFORMATION

Corresponding Author

Christopher M. Evans — Department of Materials Science and Engineering, University of Illinois at Urbana-Champaign, Urbana, Illinois 61801, United States; Beckman Institute for Advanced Science and Technology, University of Illinois at Urbana-Champaign, Urbana, Illinois 61801, United States; orcid.org/0000-0003-0668-2500; Email: cme365@illinois.edu

Author

Qiujie Zhao — Department of Materials Science and Engineering, University of Illinois at Urbana-Champaign, Urbana, Illinois 61801, United States

Complete contact information is available at: https://pubs.acs.org/10.1021/acs.macromol.0c02801

Notes

The authors declare no competing financial interest.

ACKNOWLEDGMENTS

This work is funded by the National Science Foundation (NSF) under award DMR-1751291. Part of the research was carried out in the Materials Research Laboratory (MRL), the

Microanalysis Laboratory, and the NMR Laboratory at the University of Illinois, Urbana-Champaign. We are grateful to Dr. Roddel Remy and Dr. Mohammad Amdad Ali at MRL for instrument support and Dr. Wei Lu from Tosoh for SEC measurements.

REFERENCES

- (1) Ohno, H. Electrochemical Aspects of Ionic Liquids; John Wiley & Sons, Inc.: Hoboken, N.J., 2005.
- (2) Mecerreyes, D. Polymeric ionic liquids: Broadening the properties and applications of polyelectrolytes. *Prog. Polym. Sci.* **2011**, *36*, 1629–1648.
- (3) Ford, H. O.; Merrill, L. C.; He, P.; Upadhyay, S. P.; Schaefer, J. L. Cross-Linked Ionomer Gel Separators for Polysulfide Shuttle Mitigation in Magnesium—Sulfur Batteries: Elucidation of Structure—Property Relationships. *Macromolecules* **2018**, *51*, 8629—8636.
- (4) Inceoglu, S.; Rojas, A. A.; Devaux, D.; Chen, X. C.; Stone, G. M.; Balsara, N. P. Morphology—Conductivity Relationship of Single-Ion-Conducting Block Copolymer Electrolytes for Lithium Batteries. *ACS Macro Lett.* **2014**, *3*, 510–514.
- (5) Peng, X.; Liu, H.; Yin, Q.; Wu, J.; Chen, P.; Zhang, G.; Liu, G.; Wu, C.; Xie, Y. A zwitterionic gel electrolyte for efficient solid-state supercapacitors. *Nat. Commun.* **2016**, *7*, 11782.
- (6) Kim, T. Y.; Lee, H. W.; Stoller, M.; Dreyer, D. R.; Bielawski, C. W.; Ruoff, R. S.; Suh, K. S. High-Performance Supercapacitors Based on Poly(ionic liquid)-Modified Graphene Electrodes. *ACS Nano* **2010**, *5*, 436–442.
- (7) Qiu, B.; Lin, B.; Si, Z.; Qiu, L.; Chu, F.; Zhao, J.; Yan, F. Bisimidazolium-based anion-exchange membranes for alkaline fuel cells. *J. Power Sources* **2012**, *217*, 329–335.
- (8) Gu, Y.; Lodge, T. P. Synthesis and Gas Separation Performance of Triblock Copolymer Ion Gels with a Polymerized Ionic Liquid Mid-Block. *Macromolecules* **2011**, *44*, 1732–1736.
- (9) Bara, J. E.; Gabriel, C. J.; Hatakeyama, E. S.; Carlisle, T. K.; Lessmann, S.; Noble, R. D.; Gin, D. L. Improving CO2 selectivity in polymerized room-temperature ionic liquid gas separation membranes through incorporation of polar substituents. *J. Membr. Sci.* **2008**, *321*, 3–7.
- (10) Bara, J. E.; Hatakeyama, E. S.; Gabriel, C. J.; Zeng, X.; Lessmann, S.; Gin, D. L.; Noble, R. D. Synthesis and light gas separations in cross-linked gemini room temperature ionic liquid polymer membranes. *J. Membr. Sci.* **2008**, *316*, 186–191.
- (11) Nikolaeva, D.; Azcune, I.; Sheridan, E.; Sandru, M.; Genua, A.; Tanczyk, M.; Jaschik, M.; Warmuzinski, K.; Jansen, J. C.; Vankelecom, I. F. J. Poly(vinylbenzyl chloride)-based poly(ionic liquids) as membranes for CO2 capture from flue gas. *J. Mater. Chem. A* **2017**, *5*, 19808–19818.
- (12) Zhao, F.; Meng, Y.; Anderson, J. L. Polymeric ionic liquids as selective coatings for the extraction of esters using solid-phase microextraction. *J. Chromatogr. A* **2008**, 1208, 1–9.
- (13) Kohno, Y.; Gin, D. L.; Noble, R. D.; Ohno, H. A thermoresponsive poly(ionic liquid) membrane enables concentration of proteins from aqueous media. *Chem. Commun.* **2016**, *52*, 7497–7500.
- (14) Shen, C.; Zhao, Q.; Evans, C. M. Precise Network Polymerized Ionic Liquids for Low-Voltage, Dopant-Free Soft Actuators. *Adv. Mater. Technol.* **2019**, *4*, 1800535.
- (15) Kim, O.; Kim, H.; Choi, U. H.; Park, M. J. One-volt-driven superfast polymer actuators based on single-ion conductors. *Nat. Commun.* **2016**, *7*, 13576.
- (16) Green, M. D.; Wang, D.; Hemp, S. T.; Choi, J.-H.; Winey, K. I.; Heflin, J. R.; Long, T. E. Synthesis of imidazolium ABA triblock copolymers for electromechanical transducers. *Polymer* **2012**, *53*, 3677–3686.
- (17) Dong, Y.; Yin, J.; Zhao, X. Microwave-synthesized poly(ionic liquid) particles: a new material with high electrorheological activity. *J. Mater. Chem. A* **2014**, *2*, 9812–9819.

- (18) Choi, U. H.; Ye, Y.; Salas de la Cruz, D.; Liu, W.; Winey, K. I.; Elabd, Y. A.; Runt, J.; Colby, R. H. Dielectric and Viscoelastic Responses of Imidazolium-Based Ionomers with Different Counterions and Side Chain Lengths. *Macromolecules* **2014**, *47*, 777–790.
- (19) Iacob, C.; Matsumoto, A.; Brennan, M.; Liu, H.; Paddison, S. J.; Urakawa, O.; Inoue, T.; Sangoro, J.; Runt, J. Polymerized Ionic Liquids: Correlation of Ionic Conductivity with Nanoscale Morphology and Counterion Volume. *ACS Macro Lett.* **2017**, *6*, 941–946.
- (20) Choi, U. H.; Lee, M.; Wang, S.; Liu, W.; Winey, K. I.; Gibson, H. W.; Colby, R. H. Ionic Conduction and Dielectric Response of Poly(imidazolium acrylate) Ionomers. *Macromolecules* **2012**, *45*, 3974–3985.
- (21) Bartels, J.; Sanoja, G. E.; Evans, C. M.; Segalman, R. A.; Helgeson, M. E. Decoupling Mechanical and Conductive Dynamics of Polymeric Ionic Liquids via a Trivalent Anion Additive. *Macromolecules* **2017**, *50*, 8979–8987.
- (22) la Cruz, D. S.-d.; Green, M. D.; Ye, Y.; Elabd, Y. A.; Long, T. E.; Winey, K. I. Correlating backbone-to-backbone distance to ionic conductivity in amorphous polymerized ionic liquids. *J. Polym. Sci., Part B: Polym. Phys.* **2012**, *50*, 338–346.
- (23) Fan, F.; Wang, Y.; Hong, T.; Heres, M. F.; Saito, T.; Sokolov, A. P. Ion Conduction in Polymerized Ionic Liquids with Different Pendant Groups. *Macromolecules* **2015**, *48*, 4461–4470.
- (24) Kuray, P.; Noda, T.; Matsumoto, A.; Iacob, C.; Inoue, T.; Hickner, M. A.; Runt, J. Ion Transport in Pendant and Backbone Polymerized Ionic Liquids. *Macromolecules* **2019**, *52*, 6438–6448.
- (25) Evans, C. M.; Bridges, C. R.; Sanoja, G. E.; Bartels, J.; Segalman, R. A. Role of Tethered Ion Placement on Polymerized Ionic Liquid Structure and Conductivity: Pendant versus Backbone Charge Placement. ACS Macro Lett. 2016, 5, 925–930.
- (26) Chen, H.; Choi, J.-H.; Salas-de la Cruz, D.; Winey, K. I.; Elabd, Y. A. Polymerized Ionic Liquids: The Effect of Random Copolymer Composition on Ion Conduction. *Macromolecules* **2009**, *42*, 4809–4816
- (27) Nakamura, K.; Saiwaki, T.; Fukao, K.; Inoue, T. Viscoelastic Behavior of the Polymerized Ionic Liquid Poly(1-ethyl-3-vinyl-imidazolium bis(trifluoromethanesulfonylimide)). *Macromolecules* **2011**, *44*, 7719–7726.
- (28) Fan, F.; Wang, W.; Holt, A. P.; Feng, H.; Uhrig, D.; Lu, X.; Hong, T.; Wang, Y.; Kang, N.-G.; Mays, J.; Sokolov, A. P. Effect of Molecular Weight on the Ion Transport Mechanism in Polymerized Ionic Liquids. *Macromolecules* **2016**, *49*, 4557–4570.
- (29) Keith, J. R.; Rebello, N. J.; Cowen, B. J.; Ganesan, V. Influence of Counterion Structure on Conductivity of Polymerized Ionic Liquids. *ACS Macro Lett.* **2019**, *8*, 387–392.
- (30) Keith, J. R.; Mogurampelly, S.; Wheatle, B. K.; Ganesan, V. Influence of side chain linker length on ion-transport properties of polymeric ionic liquids. *J. Polym. Sci., Part B: Polym. Phys.* **2017**, *55*, 1718–1723.
- (31) Keith, J. R.; Ganesan, V. Ion transport in backbone-embedded polymerized ionic liquids. *J. Chem. Phys.* **2019**, *151*, 124902.
- (32) Keith, J. R.; Mogurampelly, S.; Aldukhi, F.; Wheatle, B. K.; Ganesan, V. Influence of molecular weight on ion-transport properties of polymeric ionic liquids. *Phys. Chem. Chem. Phys.* **2017**, *19*, 29134—29145.
- (33) Rubinstein, M.; Colby, R. H. *Polymer Physics*; Oxford University Press: New York, 2003.
- (34) Lee, M.; Choi, U. H.; Colby, R. H.; Gibson, H. W. Ion Conduction in Imidazolium Acrylate Ionic Liquids and their Polymers. *Chem. Mater.* **2010**, 22, 5814–5822.
- (35) Ye, Y.; Elabd, Y. A. Anion exchanged polymerized ionic liquids: High free volume single ion conductors. *Polymer* **2011**, *52*, 1309–1317.
- (36) Tang, H.; Tang, J.; Ding, S.; Radosz, M.; Shen, Y. Atom transfer radical polymerization of styrenic ionic liquid monomers and carbon dioxide absorption of the polymerized ionic liquids. *J. Polym. Sci., Part A: Polym. Chem.* **2005**, *43*, 1432–1443.
- (37) He, X.; Yang, W.; Pei, X. Preparation, Characterization, and Tunable Wettability of Poly(ionic liquid) Brushes via Surface-

- Initiated Atom Transfer Radical Polymerization. *Macromolecules* **2008**, *41*, 4615–4621.
- (38) Mori, H.; Yahagi, M.; Endo, T. RAFT Polymerization of N-Vinylimidazolium Salts and Synthesis of Thermoresponsive Ionic Liquid Block Copolymers. *Macromolecules* **2009**, *42*, 8082–8092.
- (39) Smith, T. W.; Zhao, M.; Yang, F.; Smith, D.; Cebe, P. Imidazole Polymers Derived from Ionic Liquid 4-Vinylimidazolium Monomers: Their Synthesis and Thermal and Dielectric Properties. *Macromolecules* **2013**, *46*, 1133–1143.
- (40) Cordella, D.; Kermagoret, A.; Debuigne, A.; Jérôme, C.; Mecerreyes, D.; Isik, M.; Taton, D.; Detrembleur, C. All Poly(ionic liquid)-Based Block Copolymers by Sequential Controlled Radical Copolymerization of Vinylimidazolium Monomers. *Macromolecules* **2015**, *48*, 5230–5243.
- (41) Park, B.; Ford, H. O.; Merrill, L. C.; Liu, J.; Murphy, L. P.; Schaefer, J. L. Dual Cation Exchanged Poly(ionic liquid)s as Magnesium Conducting Electrolytes. ACS Appl. Polym. Mater. 2019, 1, 2907–2913.
- (42) He, H.; Zhong, M.; Adzima, B.; Luebke, D.; Nulwala, H.; Matyjaszewski, K. A Simple and Universal Gel Permeation Chromatography Technique for Precise Molecular Weight Characterization of Well-Defined Poly(ionic liquid)s. J. Am. Chem. Soc. 2013, 135, 4227–4230.
- (43) Weber, R. L.; Ye, Y.; Banik, S. M.; Elabd, Y. A.; Hickner, M. A.; Mahanthappa, M. K. Thermal and ion transport properties of hydrophilic and hydrophobic polymerized styrenic imidazolium ionic liquids. *J. Polym. Sci., Part B: Polym. Phys.* **2011**, *49*, 1287–1296.
- (44) Williams, S. R.; Borgerding, E. M.; Layman, J. M.; Wang, W.; Winey, K. I.; Long, T. E. Synthesis and Characterization of Well-Defined 12,12-Ammonium Ionenes: Evaluating Mechanical Properties as a Function of Molecular Weight. *Macromolecules* **2008**, *41*, 5216–5222.
- (45) Buitrago, C. F.; Bolintineanu, D. S.; Seitz, M. E.; Opper, K. L.; Wagener, K. B.; Stevens, M. J.; Frischknecht, A. L.; Winey, K. I. Direct Comparisons of X-ray Scattering and Atomistic Molecular Dynamics Simulations for Precise Acid Copolymers and Ionomers. *Macromolecules* **2015**, *48*, 1210–1220.
- (46) Hall, L. M.; Seitz, M. E.; Winey, K. I.; Opper, K. L.; Wagener, K. B.; Stevens, M. J.; Frischknecht, A. L. Ionic aggregate structure in ionomer melts: effect of molecular architecture on aggregates and the ionomer peak. *J. Am. Chem. Soc.* **2012**, *134*, 574–587.
- (47) Liu, H.; Paddison, S. J. Direct Comparison of Atomistic Molecular Dynamics Simulations and X-ray Scattering of Polymerized Ionic Liquids. *ACS Macro Lett.* **2016**, *5*, 537–543.
- (48) Nakamura, K.; Fukao, K.; Inoue, T. Dielectric Relaxation and Viscoelastic Behavior of Polymerized Ionic Liquids with Various Counteranions. *Macromolecules* **2012**, *45*, 3850–3858.
- (49) Wieland, F.; Bocharova, V.; Münzner, P.; Hiller, W.; Sakrowski, R.; Sternemann, C.; Böhmer, R.; Sokolov, A. P.; Gainaru, C. Structure and dynamics of short-chain polymerized ionic liquids. *J. Chem. Phys.* **2019**, *151*, 034903.
- (50) Shan, N.; Shen, C.; Evans, C. M. Critical Role of Ion Exchange Conditions on the Properties of Network Ionic Polymers. *ACS Macro Lett.* **2020**, *9*, 1718–1725.
- (51) Layman, J. M.; Borgerding, E. M.; Williams, S. R.; Heath, W. H.; Long, T. E. Synthesis and Characterization of Aliphatic Ammonium Ionenes: Aqueous Size Exclusion Chromatography for Absolute Molecular Weight Characterization. *Macromolecules* **2008**, *41*, 4635–4641.
- (52) Chen, S.; Funtan, A.; Gao, F.; Cui, B.; Meister, A.; Parkin, S. S. P.; Binder, W. H. Synthesis and Morphology of Semifluorinated Polymeric Ionic Liquids. *Macromolecules* **2018**, *51*, 8620–8628.
- (53) Wasserman, S. H.; Graessley, W. W. Effects of polydispersity on linear viscoelasticity in entangled polymer melts. *J. Rheol.* **1992**, *36*, 543–572.
- (54) Nichetti, D.; Manas-Zloczower, I. Viscosity model for polydisperse polymer melts. *J. Rheol.* **1998**, 42, 951–969.
- (55) Struglinski, M. J.; Graessley, W. W. Effects of polydispersity on the linear viscoelastic properties of entangled polymers. 1.

Experimental observations for binary mixtures of linear polybutadiene. *Macromolecules* **1985**, *18*, 2630–2643.

- (56) Llorens, J.; Rudé, E.; Marcos, R. M. Polydispersity index from linear viscoelastic data: unimodal and bimodal linear polymer melts. *Polymer* **2003**, *44*, 1741–1750.
- (57) Leibler, L.; Rubinstein, M.; Colby, R. H. Dynamics of reversible networks. *Macromolecules* **1991**, 24, 4701–4707.
- (58) Chen, Q.; Tudryn, G. J.; Colby, R. H. Ionomer dynamics and the sticky Rouse model. J. Rheol. 2013, 57, 1441–1462.
- (59) Zhao, Q.; Shen, C.; Halloran, K. P.; Evans, C. M. Effect of Network Architecture and Linker Polarity on Ion Aggregation and Conductivity in Precise Polymerized Ionic Liquids. *ACS Macro Lett.* **2019**, *8*, 658–663.
- (60) Lee, J.; Lau, V. M.; Ren, Y.; Evans, C. M.; Moore, J. S.; Sottos, N. R. Effect of Polymerized Ionic Liquid Structure and Morphology on Shockwave Energy Dissipation. *ACS Macro Lett.* **2019**, *8*, 535–539.
- (61) Xiao, D.; Hines, L. G.; Li, S.; Bartsch, R. A.; Quitevis, E. L.; Russina, O.; Triolo, A. Effect of Cation Symmetry and Alkyl Chain Length on the Structure and Intermolecular Dynamics of 1,3-Dialkylimidazolium Bis(trifluoromethanesulfonyl)amide Ionic Liquids. *J. Phys. Chem. B* **2009**, *113*, 6426–6433.